Improvement of Soil Properties Maps using an Iterative Residual Correction Method

Chengcheng Xu[1], Elia Scudiero[23], Ray Anderson[32], Nathaniel Chaney[1]

[1] Department of Civil and Environmental Engineering, Duke University, Durham, NC 27705, USA

[2] Department of Environmental Sciences, University of California Riverside, Riverside, CA 92521, USA

[3] United States Department of Agriculture – Agricultural Research Service, George E. Brown Jr. Salinity Laboratory, Agricultural Water Efficiency and Salinity Research Unit, Riverside, CA 92507, USA

Correspondence to: Chengcheng Xu (Chengcheng.xu@duke.edu)

Short Summary

Accurate soil information is vital. This study developed a method to improve existing probabilistic soil maps — spatially continuous maps providing prior estimates — by correcting their probability distributions as new soil data emerges. By iteratively adjusting previous predictions, the method increases both accuracy and certainty of soil maps. Its application in California enhanced predictions for several soil properties. This method can be further used for more soil properties and regions.

Abstract

Accurate mapping of soil properties is vital for many applications, yet existing models for digital soil maps often underestimate their spatial variability or prediction uncertainties,

which introduces risk for applications such as irrigation and drainage management. This study introduces an approach — iterative residual correction (IRC) — to update existing probabilistic soil maps when new soil observations become available. We demonstrated its application for enhanced soil mapping performance using a Californian case study. To implement this, we first generate prior probabilistic soil property maps using a pruned hierarchical Random Forest (pHRF) method. These prior estimates are then refined by integrating additional soil profile data and iteratively adjusting residuals of distribution of soil properties (reducing differences between observations and prior predictions) pixel by pixel. For this purpose, we employed Random Forest regressors to gradually adjust the soil property distributions and incrementally correct prior bias. Updated soil maps were evaluated over California and at 1-km resolution to test the methodology, using additional soil observations from the World Soil Information Service, the Soil Characterization Database, the University of California Riverside, and the United States Department of Agriculture Agricultural Research Service. Posterior soil texture predictions achieved an RMSE below 10, a 7% relative reduction in errors (mass fraction of the fine-earth fraction) over priors. RMSE and spatial representation for soil organic matter and bulk density also improved. Furthermore, the method reduced prediction uncertainties (narrower prediction intervals compared to the priors) and enforced physical constraints on soil property bounds. Looking forward, this IRC method offers a scalable pathway to improve existing probabilistic soil maps, providing a strategy for the evolution of digital soil products as new soil observations emerge.

1 Introduction

Soils play an important role in regulating Earth's water, energy, and nutrient cycles (Vereecken et al., 2016). Soil maps guide agricultural practices, ecosystem management, hydraulic modeling, and climate studies, such as crop modeling, flood risk assessment, groundwater management, and climate change (Vereecken et al., 2022). The importance of soil maps has increased with the advent of precision agriculture, including site-specific seeding, irrigation, and fertilization recommendations that intrinsically depend on high-resolution soil properties (Jiang et al., 2011; Li et al., 2019; Mueller et al., 2001; Ortuani et al., 2016). However, the accuracy and reliability of these management actions heavily depend on the quality of soil maps as a critical decision-making input. Traditional soil surveys involve field observations, laboratory analyses, and expert interpretation, but are labor-intensive and expensive (Grunwald et al., 2011; Rossiter et al., 2022; Soil Survey Staff et al., 2023). These limitations have driven the development of digital soil mapping (DSM) techniques. DSM leverages decades of soil data collection and sharing, establishing quantitative models to generate georeferenced soil maps (McBratney et al., 2003).

Digital soil maps are typically derived from existing soil surveys, geostatistical models, machine learning, or hybrid approaches. Soil survey-based soil mapping method, which use low, high, and representative values to describe soil property distributions for each soil component (Soil Survey Staff et al., 2023). The method typically approximates each soil component as a triangular distribution (Chaney et al., 2016; Soil survey staff, 2023), potentially oversimplifying multi-modal distributions of soil properties in some cases

(Haghverdi et al., 2020; Nussbaum et al., 2023). Additionally, estimating soil properties from synthetic sampling within a map unit could create artificial spatial patterns, adding noises into the mapping results (Chaney et al., 2019). Developments such as Latin-hypercube sampling and landscape adaptive covariance functions have improved the representation of spatial patterns of soil properties (Minasny and McBratney, 2006). Yet, soil survey-based approaches remain valuable particularly in areas where soil profile data is limited (Nauman et al., 2024). Geostatistical models often require presumed parameterization and are constrained by stationarity assumptions, which is difficult to apply in areas with insufficient field knowledge (Oliver and Webster, 2014). To address these challenges, non-parametric models, such as Random Forest, trained with hybridized soil data that combine soil surveys with georeferenced soil profiles show potentials in improving soil mapping, particularly for large-scale maps (Chaney et al., 2019; Nauman et al., 2024).

Map of soil properties have been observed with bias compared to field observations in certain areas due to many factors (Hengl et al., 2017; Powers et al., 2011). At the measurement level, sampling methods may favor certain landscape positions or soil conditions, causing a clustered representation (Ramcharan et al., 2018). In areas with coarse sampling density, models trained on unrepresentative data are likely to deviate from actual observations (Sharififar et al., 2019). Commonly used DSM models can show bias. For example, Random Forest classifier favors the majority class (Chen et al., 2004), and Random Forest regressors struggle to capture extreme values (Nauman et al., 2024).

Furthermore, certain areas may not be fully captured by the DSM model and the selected feature space, such as areas with complex glacial pattern, parent material transitions, and alluvial processes (unaddressed problem in SOLUS; SoilGrids 2.0; (Nauman et al., 2024; Poggio et al., 2021)). Model-based solutions include using ensemble models to enhance accuracy compared to a single model (Sylvain et al., 2021). Post-processing methods, such as regression kriging and bias-corrected decision trees, can also be used (Hengl et al., 2004). Yet, kriging-based methods have limitations in areas with high spatial heterogeneity and abrupt transitions, where stationary assumptions do not meet. Non-parametric models can be used for bias correction that overcome the limitation of making presumed distributions.

Quantifying uncertainties in DSM is important for its practical applications (Schmidinger and Heuvelink, 2023). DSM products represent soil properties as multi-dimensional matrices showing vertical and horizontal soil variation (Vereecken et al., 2022), with each pixel containing weighted possible values and their prediction uncertainties. These uncertainties can be represented either as continuous values through prediction intervals or as discrete classifications with associated class probabilities (Chaney et al., 2016, 2019; Hengl et al., 2017; Ramcharan et al., 2018). Common quantification approaches include geostatistical techniques like kriging, where the nugget term accounts for measurement errors while kriging variance reflects spatial uncertainty patterns (Chilès and Delfiner, 2012; Takoutsing et al., 2022), and machine learning methods such as Quantile Random Forest (QRF) which generates probability distributions from decision tree outputs

111 using values of soil properties (Poggio et al., 2021; Shi et al., 2024). For discrete
112 classifications, uncertainty derives from soil raster probabilities during soil taxa
113 classification (Chaney et al., 2016; Odgers et al., 2015). Given the data-driven nature of
114 DSM and frequent limitations in soil profile availability, integrating multiple qualified data
115 sources improves the amount of soil data and reduce prediction uncertainties (Nauman et
116 al., 2024), particularly in regions where predictions must rely more heavily on legacy soil
117 data.
118
119 In this study, we present a hybrid DSM approach combining pruned Hierarchical Random
120 Forest (pHRF) with iterative residual correction (IRC) method (Xu et al., 2025). The pHRF
121 method leverages the National Cooperative Soil Survey (NCSS) soil survey data and
122 georeferenced soil taxa information to generate prior distributions, while additional soil
123 profiles correct biases in prior predictions. This method builds on development in previous
124 research while addressing specific limitations. Sylvain et al. (2021) applied XGBoost
125 (sequential decision trees) and ensemble models to correct deterministic soil property
126 maps, demonstrating reduced bias for many soil properties (Sylvain et al., 2021). Zhang et
127 al. (2010) introduced a bias-correction technique with Random Forest models to mitigate
128 their tendency to regress toward mean values, though not in DSM contexts (Zhang and Lu,
129 2012). Our approach extends these concepts by probabilistically updating posterior
130 distributions at each location through an iterative correction process that continues until
131 convergence across vertical intervals. Vertical correlations are maintained through layer-
132 by-layer residual correction, which preserves inter-layer correlations while dynamically

optimizing the feature space at each correction step. Unlike methods requiring distributional assumptions, our non-parametric framework adapts to diverse landscapes and data scenarios. The models implement residual correction by minimizing the differences between priors and new observations to adjust posterior distributions, with the entire process continuing until property variations stabilize between different iterations. This method aims to improve the accuracy and reliability of soil property maps, supporting decision-making in relevant applications.

2 Methods

This study introduces a hybrid framework for digital soil mapping (DSM) that updates existing probabilistic soil property maps using newly collected soil observations. The framework combines prior soil property estimates with an iterative residual correction (IRC) method. The IRC method integrates additional georeferenced soil profiles (soil observations not used to train prior soil maps) and employs non-parametric models to adjust the distribution of prior estimates, thereby correcting biases in the prior soil maps.

The following sections first describe the general residual correction framework (Section 2.1). To illustrate the method concretely, we then provide a worked example using one randomly selected soil column to demonstrate how the feature space is constructed and updated across two consecutive iterations (Section 2.1.1). Building on this example, we detail the key components of the IRC method: the iterative update of feature space (Section 2.1.2), the convergence criteria for residual correction (Section 2.1.3), and the

process for updating posterior soil properties with physical constraints (Section 2.1.4). Finally, we present the California case study (Section 2.2), describing the soil datasets used (Section 2.2.1) and the implementation details for applying the IRC method over California (Section 2.2.2).

2.1 Iterative Residual Correction Framework for DSM

Residual correction is implemented to address underestimated soil property variation in prior maps (tendency to underestimate high values and overestimate low values, smoothing out soil variation across landscape). The overall workflow of the IRC method consists of three components: (1) prior map generation (Figure 1a), (2) residual preparation (Figure 1b), and (3) iterative correction (Figure 1c).

First, probabilistic prior soil property maps are generated or retrieve probabilistic soil property maps from an existing DSM product as the prior soil maps (Figure 1a). These maps represent the initial estimates of soil properties and their associated uncertainties. Second, a residual preparation step is carried out to enable correction using new soil profile observations (Figure 1b). The preparation involves four key steps: (1) adding additional soil profiles from new field measurements or databases; (2) spatially aligning these profiles with the corresponding pixels in the prior soil maps using geographic coordinates; (3) vertically aligning observations with prior predictions at matching depth intervals; and (4) calculating residuals depth by depth as the difference between observed values and prior predictions. During this stage, the feature space for residual modeling is

also prepared, consisting of static environmental covariates (which remain fixed throughout iterations) and dynamic soil covariates (which are updated iteratively). Detailed construction of the feature space is described in Section 2.1.1.

Finally, iterative residual correction is performed to update soil property estimates across depths (Figure 1c). During each iteration, the model predicts residuals for one depth layer at a time, with the layer selected randomly. A Random Forest regressor is trained to learn the relationship between residuals and the feature space at sampled locations, then interpolates residual corrections across the study area. Predicted residuals are added to the prior (or previous iteration's) estimates to generate updated soil property values. After each update, convergence is evaluated for the modeling depth by comparing the median difference between the current residuals and those from the previous iteration. Once this change falls below a predefined threshold, that depth is considered converged and excluded from subsequent updates. The algorithm then focuses on the remaining "unconverged" depths, until convergence is achieved across all layers. After convergence is verified for all depths, the final corrected residuals are added to the prior estimates to update the posterior distributions of soil properties.

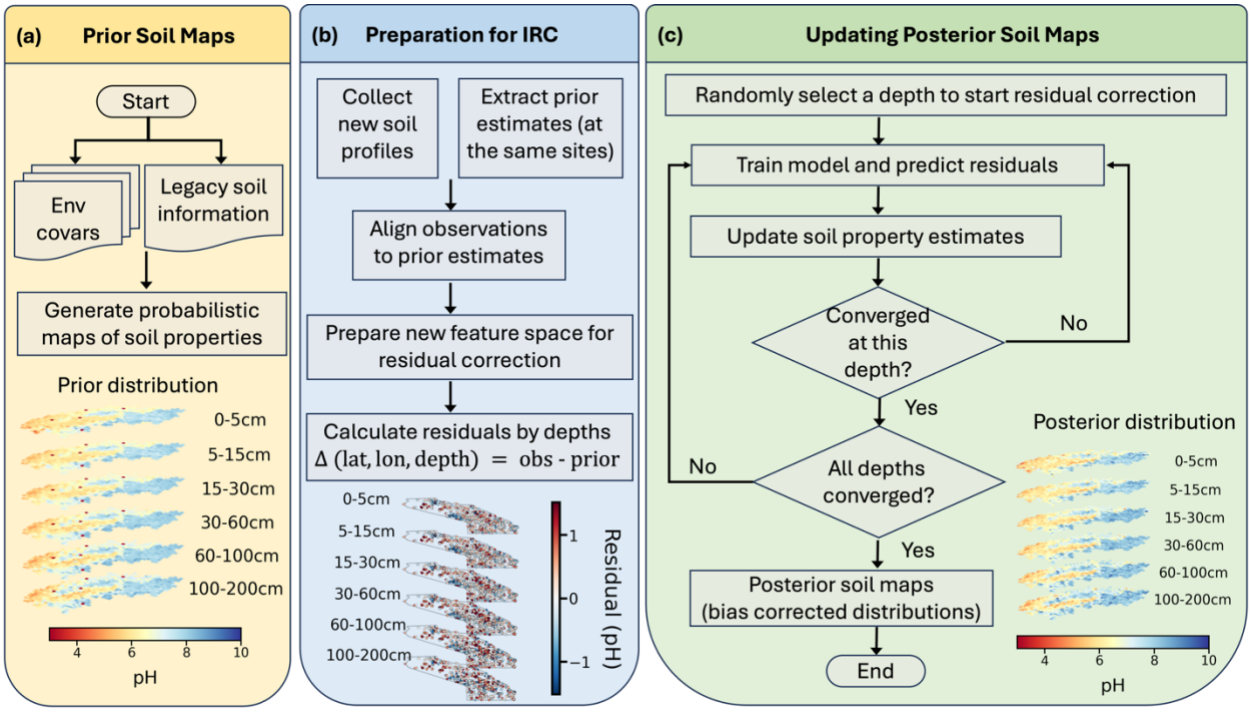

Figure 1: Workflow for updating posterior soil property maps. The process begins with panel (a), the preparation of environmental covariates (env covars) to generate probabilistic maps of soil properties (prior soil maps). As illustrated in panel (b), the preparation for residual correction involves adding additional soil profiles, spatially and vertically aligning prior soil map values with new profile observations, calculating residuals depth by depth, and preparing environmental covariates and soil covariates (new feature space) for residual correction. Finally, as shown in panel (c), the iterative residual correction step applies bias corrections across different depths, focusing on layers where residuals have not yet stabilized. During each iteration, the model predicts residuals for one depth at a time, randomly selecting a layer. Once residuals for a given depth converge, that layer is excluded from further updates, allowing the model to concentrate on remaining depths until all achieve stability. After verifying convergence across all depths,

the algorithm updates the posterior distribution of soil properties and produces the final soil maps (posterior soil property maps).

In this IRC framework, "prior probabilistic soil property maps" refer to spatially continuous soil property maps that provide an initial (prior) estimate of soil properties with associated uncertainty across the study area. These prior maps provide, for each pixel and depth interval, a distribution of possible soil property values with associated probabilities or weights. The IRC method does not require prior and new soil observations to be co-located at the same pixels. Instead, the method requires that a prior estimate exists at locations where new soil observations are available. By learning the relationship between residuals (differences between new observations and prior estimates) and environmental and soil covariates at sampled locations, the trained model can interpolate residual corrections across the study area.

2.1.1 Worked Example

The iterative residual correction method is further illustrated in Figure 2 using an example with a randomly selected soil column. Figure 2a shows the location of the selected soil column, where additional soil profile observations are available. The right panel displays the top-3 probable pH values (from prior soil maps) at each depth intervals (0–5 cm, 5–15 cm, 15–30 cm, 30–60 cm, 60–100 cm, 100–200 cm), while the left panel shows the three weights (probabilities) associated with these pH values. In this simplified example, we use 3 bins to represent the soil property distribution; however, in actual implementation, more

bins are maintained (typically top-12 probable values) to better capture soil variability. For this demonstration, Depth 2 (D_2; 5–15 cm) is randomly selected as the modeling layer to initiate the iterative correction process. Only one layer is modeled and updated for a given iteration. Note that in real model execution, model generally processes over 3,000 soil columns simultaneously in California, though only one column is shown here for clarity.

In Figure 2b, the table details features used to train the Random Forest regressor for residual prediction. The feature space consists of environmental covariates that remain fixed across iterations and soil covariates that are updated iteratively:

(1) Environmental covariates (21 dimensions): These capture spatial variations in soil-forming factors and remain unchanged throughout all iterations. The covariates include remote sensing data (Sentinel-1, Sentinel-2, GOES land surface temperature) and terrain attributes, identical to those used in the prior mapping method (Xu et al., 2025).

(2) Depth information (1 dimension): The centroid (median value) of the soil depth interval for the modeling layer (e.g., 10 cm for the 5–15 cm layer), describing the vertical position in the soil profile.

(3) Representative soil property values (1 dimension): The expected value (weighted mean) of the soil property at each pixel in the modeling layer, representing the current best estimate. This is computed as the weighted sum of top-probable values.

(4) Top-probable soil property values (1 dimension): The current predictions at each pixel (residuals plus previous prediction of soil property values), reflecting both intra-pixel and inter-pixel soil heterogeneity.

(5) Inter-layer differences (5 dimensions): Differences in top-probable predicted soil property values between the modeling layer and the other five depth layers. For instance, if modeling Depth 2, the inter-layer differences would be (D_2-D_1), (D_2-D_3), (D_2-D_4), (D_2-D_5), and (D_2-D_6). These features capture vertical correlations in the soil profile and aid in estimating spatial patterns.

(6) Weights (1 dimension): Probabilities associated with each top-probable soil property value. These weights remain fixed throughout iterations.

In summary, environmental covariates and weights remain static, while depth information, representative values, top-probable values, and inter-layer differences are updated across iterations based on the most recent soil property estimates.

A Random Forest regressor is then trained using the feature space to predict residuals for the modeling layer (D_2 in this example). The right panel in Figure 2c compares the distribution of pH values before and after residual adjustment in the current iteration. After applying the residual correction, convergence is checked for D_2 by comparing the median difference between the current and previous residuals. If D_2 has converged (difference below threshold), the algorithm proceeds to check whether all depth layers have converged. If all layers have converged, the iterative process terminates, and the final

posterior soil property maps are generated by adding the last predicted residuals to the prior values.

If either convergence check returns "No" (i.e., D_2 has not converged or other layers remain unconverged), the algorithm continues iterating. Here, the soil property values for D_2 are updated by adding the predicted residuals to the previous pH values. These updated values are then used to reconstruct the feature space following the same structure described above, updating the representative values, top-probable values, and inter-layer differences. By updating soil covariates layer by layer and iteratively refining the feature space, the next prediction retains prior knowledge while integrating new information about soil heterogeneity and vertical relationships for soil profiles (Wu et al., 2025). A new iteration begins by randomly selecting another unconverged layer, and the process repeats until convergence is achieved across all depth layers.

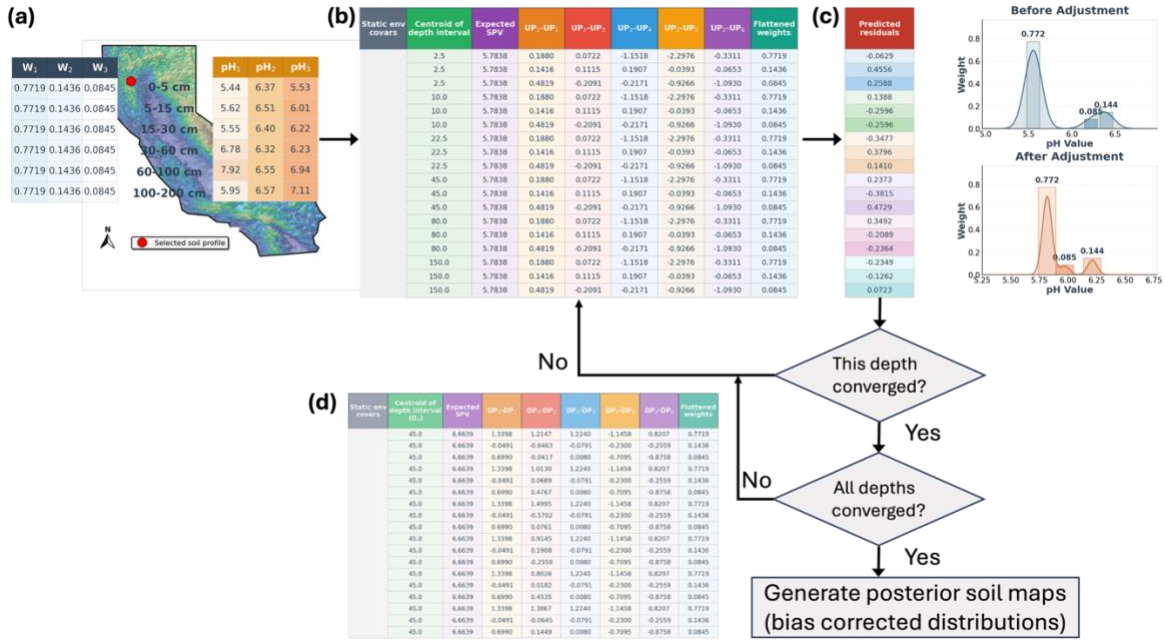

Figure 2: Schematic illustration of the iterative residual correction (IRC) method using a worked example at a randomly selected soil column. (a) Prior distributions and observation location: The map shows the location of the selected soil column within the study area. The right panel displays the top-3 probable pH values at each of the six depth intervals (0–5 cm, 5–15 cm, 15–30 cm, 30–60 cm, 60–100 cm, 100–200 cm), while the left panel shows the three weights (w_1, w_2, w_3) associated with these pH values. Depth 2 (D_2; 5–15 cm) is randomly selected for this iteration. (b) Feature space components: The table details the structure of the feature space used to train the Random Forest regressor for residual prediction. The feature space comprises both static and dynamic components. Static components include environmental covariates (satellite imagery, terrain attributes) that remain unchanged throughout iterations, and weights (w_1, w_2, w_3) associated with top-probable values. Dynamic soil covariates that are updated in each iteration include: the centroid of the depth interval (e.g., 10 cm for D_2), the expected (representative) soil

property value computed as the weighted mean, the top-probable soil property values reflecting intra-pixel heterogeneity, and inter-layer differences capturing vertical correlations (e.g., D_2-D_1, D_2-D_3). (c) Residual correction and convergence workflow: A Random Forest model trained on the feature space predicts residuals for the modeling layer D_2. The right panel compares the pH distribution before and after residual adjustment. The flowchart below describes the convergence logic: after predicting and applying residuals to D_2, the algorithm evaluates whether D_2 has converged. If D_2 has converged, the algorithm checks whether all depth layers have achieved convergence. If both checks pass, the final posterior soil property maps are generated by adding the last converged residuals to the prior values. (d) If either check fails, the algorithm updates the soil property values for D_2 by adding predicted residuals, reconstructs the feature space with the updated values, randomly selects another unconverged layer, and repeats the process. This iterative cycle continues until convergence is achieved across all six depth layers.

2.1.2 Convergence of Residual Correction

The residual correction process continues until the median difference between updated residuals and previous residuals falls below a predefined threshold. Convergence is achieved when the residuals stabilize across multiple iterations, indicating that further adjustments do not largely change the predictions. This stability ensures that the final posterior soil properties are reliable and consistent. The stopping criterion is a customizable parameter. In this work, it was set to the 5th percentile of the distribution of

value changes. To avoid over-correcting bias, only the last converged residuals are added to the prior prediction to generate the final posterior results.

2.1.3 Update with Constraints

During residual correction, a common issue arises where the addition of residuals to prior soil property values results in values that exceed physical bounds (such as sand content > 100%; fine-earth fraction in mass). To address this, a residual update process with constraints is implemented.

As illustrated in Figure 2c to 2d, after the Random Forest regressor predicts residuals for the layer (D_2), these residuals are added to the previous soil property values to generate updated predictions. Immediately after this addition step, the updated values are examined to check whether they fall within predefined physical bounds (e.g., 0% to 100% for particle size fractions, positive values for bulk density). This constraint check occurs before the convergence evaluation and before the updated values are used to reconstruct the feature space for the next iteration.

If any updated value exceeds the physical bounds, it is adjusted to the nearest valid bound (minimum or maximum). For example, if adding a residual of +15% to a prior sand content of 90% yields 105%, this value is capped at 100% (mass fraction). The "excess" residual (+5% in this case) is then redistributed proportionally (based on their weights) among the other top-probable values at the same pixel, ensuring that the total correction remains

consistent with the model's prediction while maintaining physical plausibility. For particle size fractions (sand, silt, clay), an additional compositional constraint ensures that the three fractions sum to 100% at each pixel after residual correction.

2.2 California Case Study: Soil Data and Model Implementation

2.2.1 Soil Data

To demonstrate the IRC method, we apply it to soil property mapping in California. We use georeferenced soil profiles with laboratory measurements of soil properties. We compiled soil profile data from three primary sources: the World Soil Information Service (WoSIS), the National Soil Characterization Database (SCD), and field measurements conducted in California (Batjes et al., 2024; National Cooperative Soil Survey, 2018; Scudiero et al., 2024).

To ensure consistency across different data sources, we applied several quality control steps. First, we checked the physical plausibility of all soil property values by defining a valid range with specific minimum and maximum thresholds for each property. Any data point falling outside these ranges was considered an error and removed. For soil texture, we required the sum of sand, silt, and clay fractions to equal 100% (mass fraction). If a profile did not meet this compositional constraint, it was excluded. After quality check, the datasets are compatible because the WoSIS records for California are largely derived from the NCSS database, and both the SCD and WoSIS datasets follow standardized laboratory protocols, such as those from the Kellogg Soil Survey Laboratory (Soil, 1996; Soil Survey

Staff, 2014). For our own field measurements, we used the Integral Suspension Pressure (ISP+) method to maintain precision for particle size analysis (Corwin and Scudiero, 2020; Scudiero et al., 2024).

During preprocessing, we harmonized all soil data, which was originally reported at different soil horizons, into six standard depth intervals: 0–5 cm, 5–15 cm, 15–30 cm, 30–60 cm, 60–100 cm, and 100–200 cm (Arrouays et al., 2014). The harmonization was performed using equal-area spline functions to interpolate soil property values from the original horizon depths to these standard intervals (Hartemink et al., 2010, p.201). The spline function fits a smooth curve through observed values at their measured depths, then calculates the area under this curve within each standardized depth interval and divides by the interval width to obtain the value. Location of soil profiles and their distribution of soil property values are presented in Figure 3. Six soil properties are studied: sand content (% mass), silt content (% mass), clay content (% mass), pH, soil organic matter (log-scaled % mass), and oven-dry bulk density (g cm^{-3}). These samples were not co-located with the training samples used to generate the prior maps (samples at the same locations were already removed). The number of observations varies by soil property: pH has the most samples, followed by oven-dry bulk density and soil organic matter. The sample sizes across properties can also be inferred from the frequency histograms shown in the lower-left corner of each panel in Figure 3. Across all depths combined, each soil property has more than 11000 observations in California. The number of observations

388 generally decreases with depth, with depths below 1 m having notably fewer samples
389 compared to shallower layers.
390

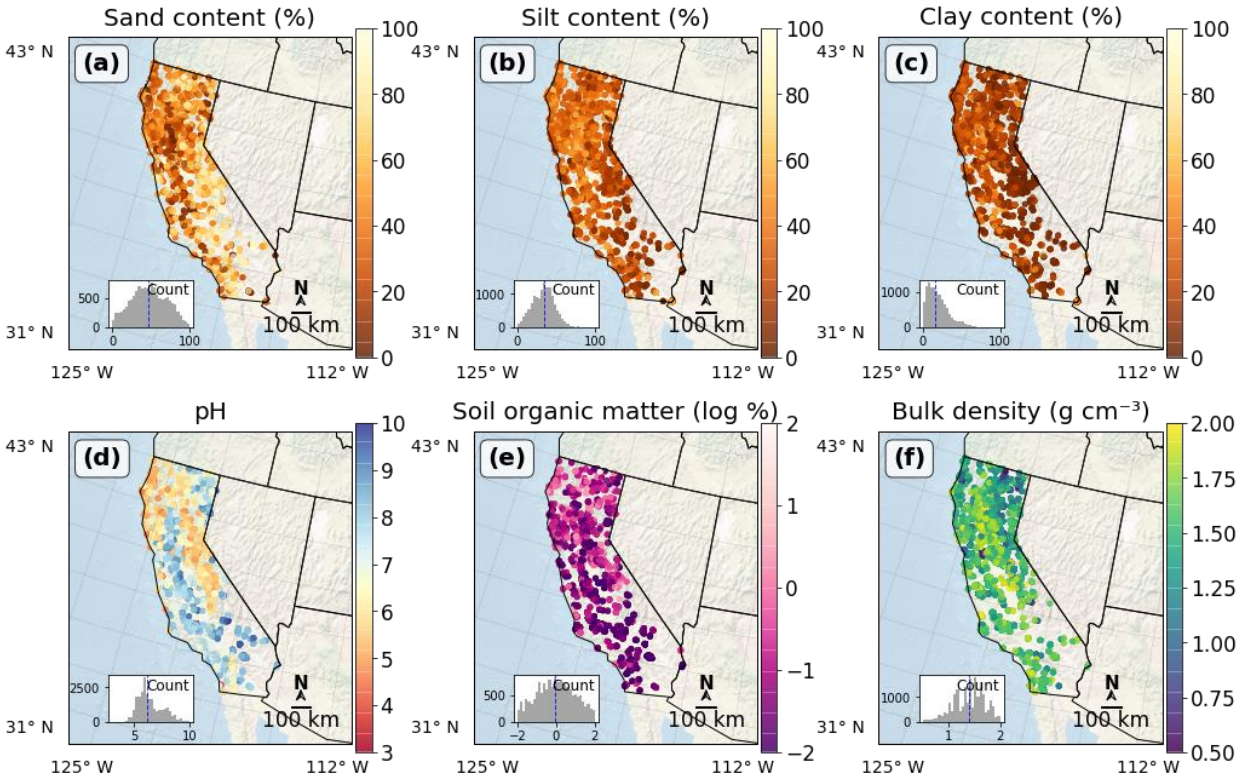

391

392 Figure 3: Spatial distribution and statistical characteristics of soil properties observations
393 across California. The figure presents six soil parameters mapped using an Albers Equal
394 Area projection: (a) sand content (% mass), (b) silt content (% mass), (c) clay content (%
395 mass), (d) pH, (e) soil organic matter (log-scaled % mass), and (f) bulk density (g cm^{-3}).
396 Each subplot displays sample locations as colored points, with field-collected samples
397 shown as triangles to distinguish them from WoSIS (circles) and SCD (squares) samples.
398 Distribution histograms in the lower left corner of each subplot show the frequency
399 distribution of values, with blue dashed lines indicating median values. Distance scale bar
400 and compass rose are provided in the right corner. Note that the total number of soil

measurements varies by property and generally decreases with depth beyond the surface layer, with the surface layers and depths below 1 m generally having fewer observations.

2.2.1.1 World Soil Information Service (WoSIS)

The World Soil Information Service (WoSIS), managed by the International Soil Reference and Information Centre (ISRIC), aggregates global soil data from diverse sources, including national soil institutes, research organizations, and collaborative initiatives like the Global Soil Partnership (GSP) and the International Network of Soil Information Institutions (INSII). The database provides soil properties for different soil horizons, georeferenced in decimal degrees, and undergoes quality controls (Batjes et al., 2024). In California, WoSIS typically offers 2,000 to over 5,000 soil observations for the modeling soil property. Samples below 1 m depth are fewer than those from shallower layers.

2.2.1.2 Soil Characterization Database (SCD)

The Soil Characterization Database (SCD) is a subset of the National Cooperative Soil Survey (NCSS) database (National Cooperative Soil Survey, 2018). It records soil properties for each soil horizon within a soil profile (pedon), including soil texture, bulk density, and water retention. In California, SCD provides between 500 and over 1,000 soil samples per layer for the studied soil property. Each soil profile is georeferenced and includes metadata such as site location, land use, and sampling methods.

2.2.1.3 Ground Truth Soil Sampling and Measurements

Additional soil sampling was conducted to complement georeferenced soil profiles in California for model training and evaluation. These data are reported in (Scudiero et al., 2024) and are briefly discussed here. Multiple fields located between Salinas and Soledad in California's Salinas Valley were selected to collect soil particle size fraction data (Figure 4). These fields, presented as red dots in Figure 4, were chosen because they were accessible, unfarmed during the sampling period, and spread across different parts of the valley.

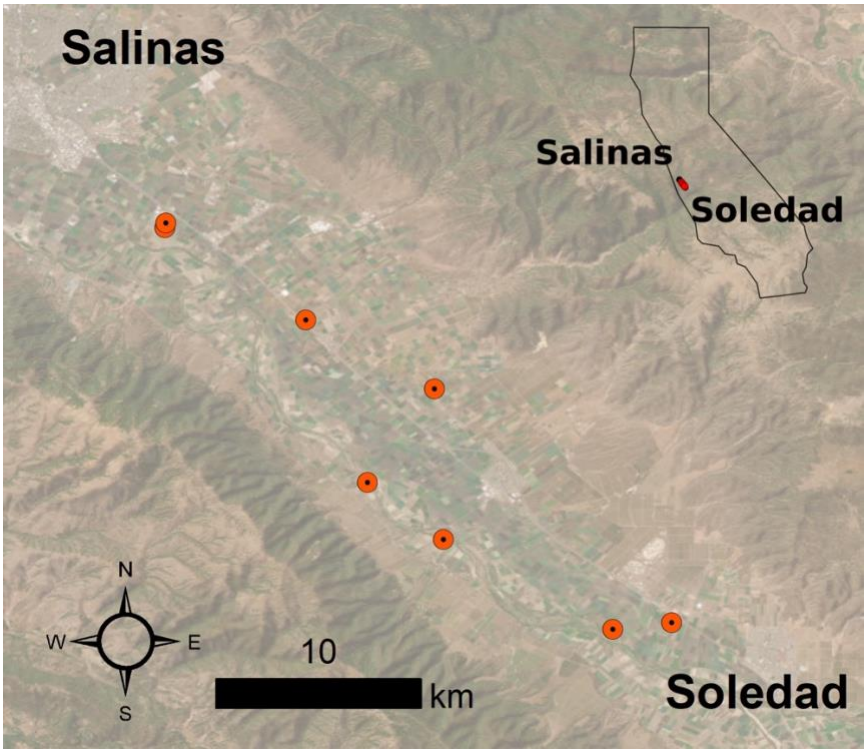

Figure 4: Map of sampling fields in the Salinas Valley in California. Each red dot represents a sampling field between Salinas and Soledad. An inset map (top right) shows the location of the sampling area within California. Scale bar and direction indicator are provided in the

left corner. *Basemap: Esri World Imagery. Source: Esri, Maxar, Earthstar Geographics, and the GIS User Community*.

Soil apparent electrical conductivity (ECa) was measured across fields using an electromagnetic induction (EMI) sensor connected to a GPS receiver. Following the ECa-directed soil sampling protocols of Corwin and Scudiero (Corwin and Scudiero, 2020), the most representative soil samples were identified with ESAP software package and the Response Surface Sampling Design algorithm (Lesch et al., 2000; Lesch, 2005). 0-0.8 and 0-1.6 m soil profiles were further analyzed and followed with the expectation that ECa was a regional proxy for the field-scale variability of particle size fraction.

To measure particle size fraction, soil samples were then collected from multiple depths (0–0.1, 0.1–0.4, and 0.4–1.2 m) across fields. After collection, the samples were air-dried, ground, and sieved to remove particles larger than 2 mm; and then measured using the Integral Suspension Pressure method (The improved integral suspension pressure method (ISP+) for precise particle size analysis of soil and sedimentary materials; Wolfgang Durner, Sascha C. Iden) using PARIO™ system (METER Group AG, Munich, Germany).

2.2.2 Model Implementation for the California Case Study

For the California case study, prior soil property maps were generated using the pruned hierarchical Random Forest (pHRF) method (Xu et al., 2025). The pHRF-derivef soil maps were developed with soil pedons from the National Soil Information System (NASIS) and

part of SCD (the remaining data not used in IRC method). After gaining prior estimate of soil properties, the IRC method was then applied using the additional soil observations from WoSIS, SCD, and field measurements, which were not used in generating the prior maps. The convergence threshold for each soil property was set to the 5th percentile of the distribution of value changes between iterations.

Model training and evaluation were performed using out-of-bag (OOB) sampling, with OOB samples (samples withheld from the training process and not used to fit the models) that shared the same geolocation as training samples removed to prevent data leakage and reduce spatial autocorrelation effects. In each iteration, a new Random Forest model is trained to update residuals for one specific depth interval, and the same set of OOB samples remains excluded throughout to ensure independent validation.

3 Results

The iterative residual correction (IRC) method is applied to adjust pHRF-derived prior soil properties, including particle size fractions (mass percentage of sand content, silt content, and clay content), pH, oven-dry bulk density (BD; $\mathrm{g\ cm^{-3}}$), and soil organic matter (SOM; log-scaled mass percentage) over California. This correction addresses biases in the prior soil property maps and updates the posterior distributions of these properties. These soil properties are important for land management and serve as essential inputs for pedotransfer functions. The residual correction is performed across California, covering six depth intervals: 0-5 cm, 5-15 cm, 15-30 cm, 30-60 cm, 60-100 cm, and 100-200 cm.

3.1 Performance Evaluation of Posterior Soil Properties

Table 1 presents the performance metrics for the posterior predictions of six key soil properties: mass percentage of sand content, silt content, and clay content (% mass), pH, oven-dry bulk density (BD; g cm^{-3}), and soil organic matter (SOM; mass percentage). The metrics include the root mean square error (RMSE), coefficient of determination (R^2), and correlation coefficient (ρ). For example, sand prediction (% mass) shows an RMSE of 9.322, an R^2 of 0.841, and a correlation coefficient of 0.918. pH prediction shows an RMSE of 0.270, an R^2 of 0.945, and a correlation coefficient of 0.972. These metrics are computed using out-of-bag (OOB) samples from random forest regressors. OOB samples are data points not included in the bootstrap samples used to train each tree in the random forest. Additionally, these metrics are evaluated by comparing the expected values of posterior predictions with co-located soil properties values; not computed on residuals.

Table 1 also shows variations in performance across different soil properties. SOM and bulk density show slightly worse metrics compared to particle size fractions and pH. For instance, SOM predictions (mass percentage) have an RMSE of 1.961, an R^2 of 0.608, and a correlation coefficient of 0.801, and bulk density predictions (g cm^{-3}) have an RMSE of 0.164, an R^2 of 0.704, and a correlation coefficient of 0.843. Two main reasons can result in their lower performance. First, these properties are more dynamic in nature compared to particle size fractions and pH. SOM and bulk density can change over time due to factors such as land use practices. The prior predictions are trained using soil survey data that are

older, while the posterior soil profiles used for evaluation may come from a different period. Second, SOM and bulk density are more challenging to model accurately. SOM is influenced by complex biological and soil-forming processes, such as decomposition rates and organic matter inputs. Similarly, bulk density is affected by soil compaction, organic matter content, and soil structure. All of them can vary spatially and temporally. Depth-wise analysis of model performance is provided in the Supplementary Information (Table S1 and S2).

Table 1: Performance metrics (RMSE, R^2, and correlation coefficient ρ) for posterior predictions of soil properties, including sand, silt, clay, pH, oven-dry bulk density (BD), and soil organic matter (SOM). The table summarizes the range (minimum and maximum values) and accuracy metrics for each property averaged across all depth intervals.

Property	Unit	Min	Max	RMSE	R^2	φ
Sand	% mass	0.0	100.0	9.322	0.841	0.918
Silt	% mass	0.0	100.0	6.556	0.788	0.889
Clay	% mass	0.0	100.0	5.891	0.841	0.918
pH	log10([H^+])	3.0	10.0	0.270	0.945	0.972
BD (oven-dry)	$g\ cm^{-3}$	0.5	2.0	0.164	0.704	0.843
SOM	% mass	0.0	100.0	1.961	0.608	0.801

The posterior predictions of soil properties all align with the co-located observations and can capture the general trend of observations (Figure 5). Predictions of pH show the most concentrated clustering to the dashed line, indicating good agreement with observations across all depths. SOM and bulk density show relatively weaker performance compared to other predicted soil properties. And this pattern of reduced accuracy persists throughout all depths.

As Figure 5 shows, the performance of the model tends to decline with increasing soil depth, except for SOM. This decline is primarily due to several reasons. First, the availability of soil data is often greater for shallower layers compared to deeper layers (such as > 1m), which limits the model's ability to learn patterns in deep layers. Second, remote sensing-derived soil covariates can only observe surface properties. Predictions for deeper layers rely on soil horizon information, soil profiles, geology, and parent material-related features. The certainty and quantity of them are less than easily measurable surface covariates. However, SOM shows better performance in deeper layers compared to surface layers. This is likely because surface SOM is highly variable due to factors like residue, land use, and management practices, while deeper SOM tends to be more stable.

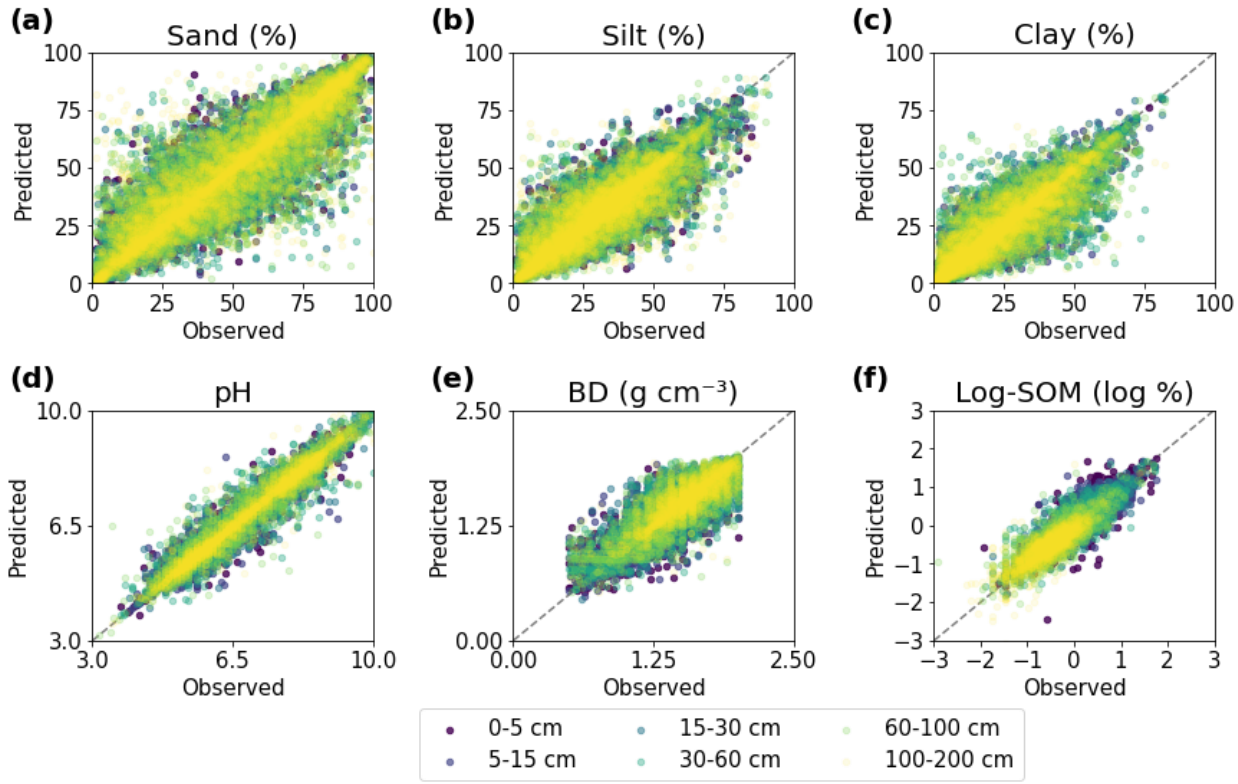

Figure 5: Evaluating posterior predictions with observations for six soil properties: (a) sand (% mass), (b) silt (% mass), (c) clay (% mass), (d) pH, (e) bulk density (BD; $\mathbf{g\ cm^{-3}}$), and (f) log-scaled soil organic matter (SOM; log % mass). The left side shows scatter plots of posterior predictions versus observations across six depth intervals, with each depth represented by a distinct color. The dashed black line represents perfect prediction.

3.2 Comparison of Prior and Posterior Soil Predictions

Prior and posterior predictions of soil properties are compared against co-located observations to assess the added value of residual correction. The radar plots in Figure 6 illustrate the improvements achieved through the residual correction method using three normalized unitless metrics: 1-normalized absolute bias (1-|Bias|), coefficient of

546 determination (R^2), and 1-normalized RMSE by ranges of soil variability (1-nRMSE). These
547 metrics are computed with values of soil properties, instead of on their residuals. Values in
548 Figure 6 closer to the outer edge of each plot indicate better model performance. Overall,
549 all soil properties maintain reasonable normalized bias and nRMSE (with nRMSE values
550 consistently less than 0.2 for both prior and posterior predictions). However, the prior
551 predictions tend to underestimate the variability of soil properties. As a result, the
552 normalized metrics for prior and posterior predictions are similar, while the R^2 values show
553 some differences.
554
555 For all soil properties, posterior predictions consistently outperform prior predictions
556 across all metrics. For particle size fractions, R^2 values show the largest improvements:
557 sand increases from 0.35 to 0.84, silt from 0.19 to 0.79, and clay from 0.25 to 0.84. The
558 nRMSE metric also shows improvements. Sand decreases from 0.19 to 0.09, silt from 0.14
559 to 0.07, and clay from 0.16 to 0.07, showing reductions in prediction errors using the
560 residual correction.
561
562 Aggregating data from all depths, Figure 6 shows the degree of improvement across
563 different soil properties. Prior pH predictions already demonstrate reasonable accuracy,
564 with an R^2 of 0.54 and nRMSE of 0.11. After the residual correction, these metrics improve
565 to 0.94 for R^2 and 0.04 for nRMSE. Bulk density and SOM show the biggest gains. For bulk
566 density, the R^2 increasing from 0.16 to 0.70 and nRMSE reducing from 0.18 to 0.11. Prior

SOM are underfitted with a low R^2 value. With the residual correction, the posterior SOM show a positive R^2 of 0.61. The nRMSE for SOM also improves from 0.07 to 0.04.

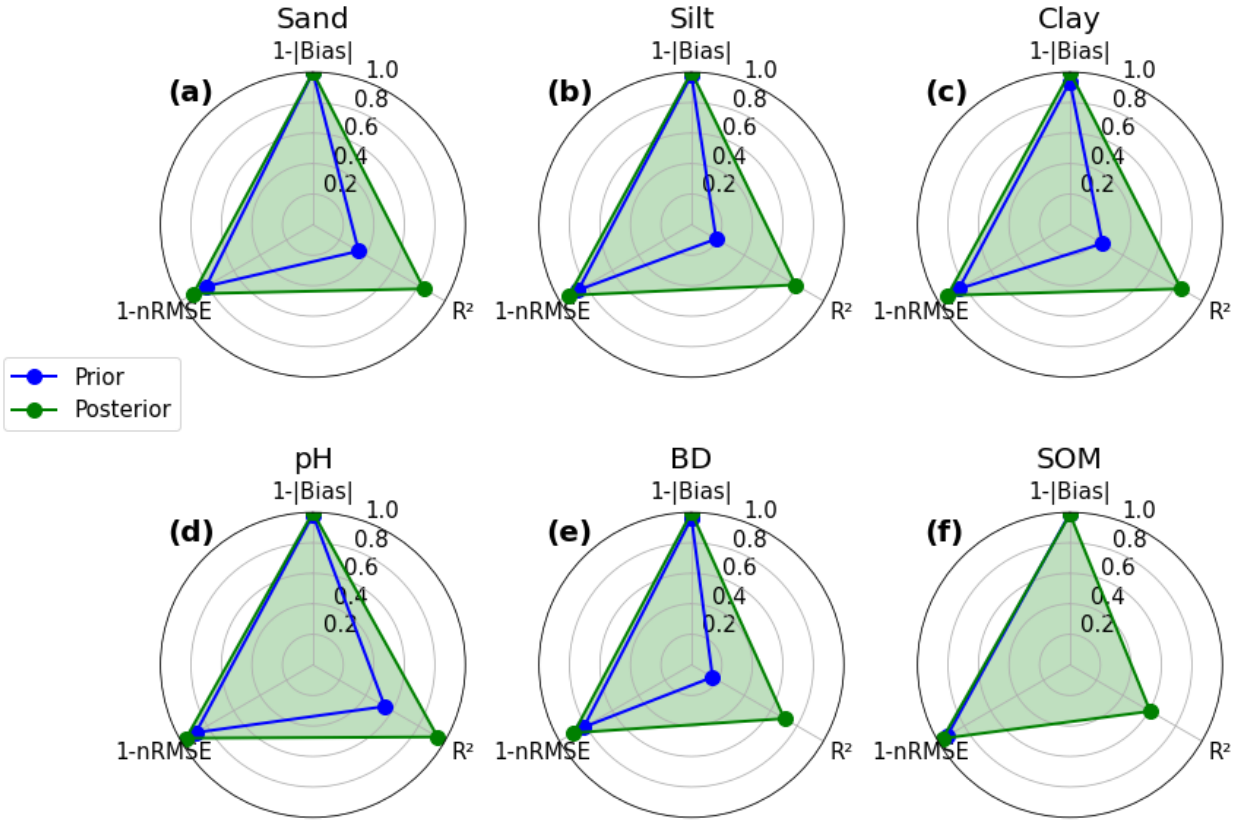

Figure 6: Radar plots comparing the performance metrics of prior and posterior predictions for six soil properties: (a) sand (% mass), (b) silt (% mass), (c) clay (% mass), (d) pH, (e) oven-dry bulk density (BD; $g\ cm^{-3}$), and (f) soil organic matter (SOM; log % mass). Each plot presents three metrics: 1-normalized absolute bias (1-|Bias|), coefficient of determination (R^2), and 1-normalized RMSE by ranges of soil variability (1-nRMSE). Prior predictions are shown in blue, and posterior predictions in green. All metrics are scaled from 0 to 1, where values closer to the outer edge of the plot indicate better model performance. The green shaded area highlights the improvement achieved by the posterior predictions over prior estimates.

579

580 Horizontal spatial patterns of the six soil properties are presented in Figure 7. In the
581 Central Valley California, soils are mostly medium textured with about 30% silt and lower
582 sand content compared to surrounding areas. In the Mojave and Colorado Deserts, high
583 sand contents (> 60% mass) with low clay contents are observed. SOM contents are also
584 low in these areas. The histograms show how residual correction adjusts the distribution of
585 soil properties.

586

587 For SOM and bulk density, the prior predictions often underestimate the observed
588 variation. Figure 7 shows that the residual correction processes add noticeable spatial
589 variations between prior and posterior soil maps. Prior bulk density values are often
590 clustered around 1.5 g cm^{-3}, whereas the posterior histogram presents a broader range,
591 spanning from 1.25 g cm^{-3} to 1.6 g cm^{-3}, capturing more heterogeneity of bulk density.
592 Similarly, the residual correction adds soil heterogeneity to SOM. The posterior SOM can
593 delineate water bodies, where SOM content is abruptly lower than the surrounding areas.
594 Additionally, the posterior SOM maps present hill features in the desert areas.

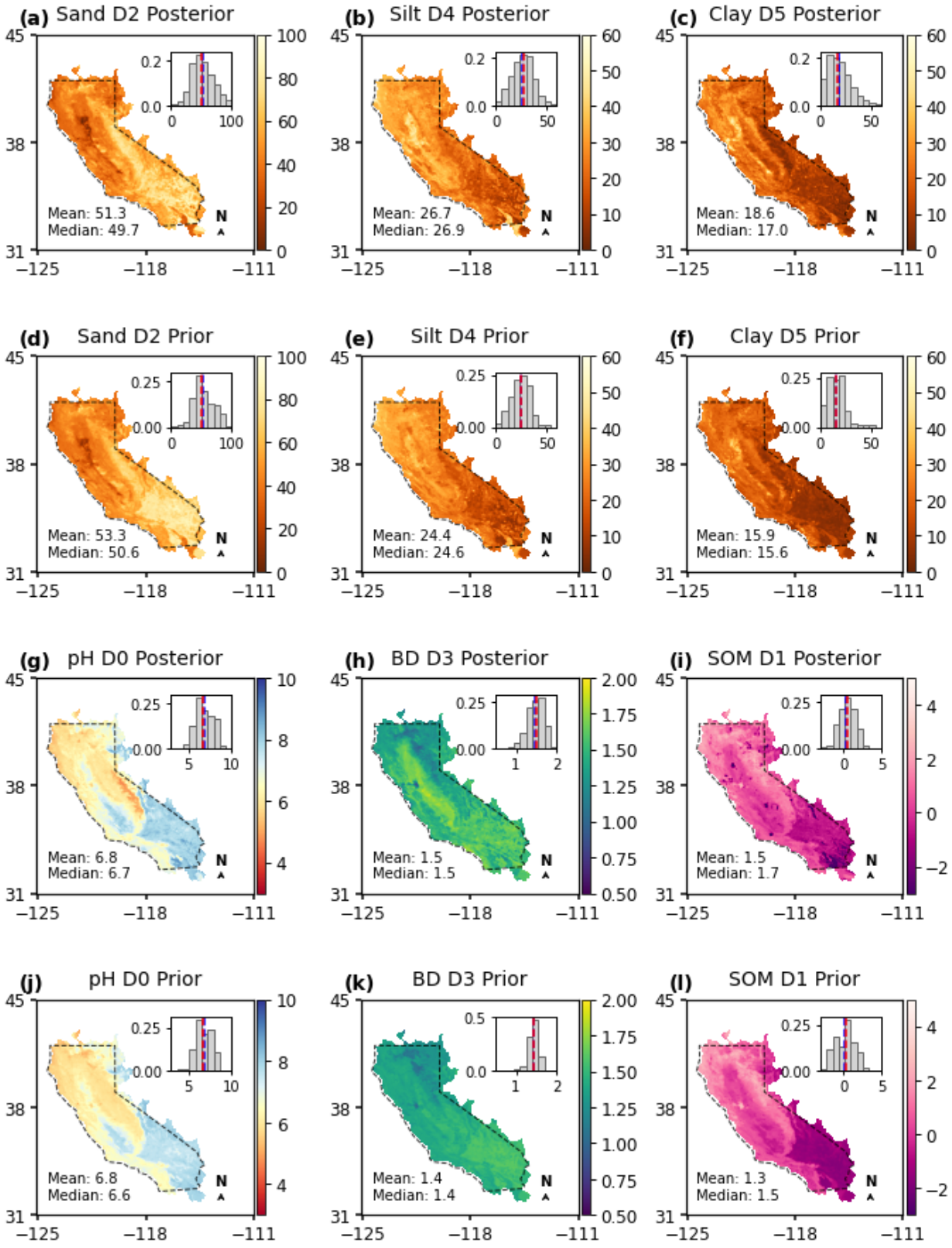

Figure 7: Spatial distribution of six soil properties: sand (% mass), silt (% mass), clay

content (% mass), pH, bulk density (g cm^{-3}), and soil organic matter (log % mass) across California. Maps of prior and posterior soil properties are compared. The corresponding frequency distributions of these soil properties are displayed in the right corner. Dashed polygons represent the continental part of California. In the histograms, the blue and red dashed lines represent the mean and median values, respectively. The maps labeled D0 to D5 correspond to the first vertical layer down to the deepest layer. Note the map and distribution of soil organic matter (SOM) is log-scaled. Mean and median values are computed from the original SOM data.

Soil profiles used for evaluating residual correction are grouped according to their corresponding pixel's land use classification from the National Land Cover Database (NLCD). Figure 8 presents selected vertical soil profiles of sand content, oven-dry bulk density, and SOM across three land use categories: forest, cultivated crops, and wetland. The number of samples varies by land use, with forests having the most, cultivated crops approximately half as many, and wetlands the fewest across California. To ensure a balanced visualization, a similar number of profiles are selected from each category. Sand content is chosen due to its broader range of variation (0-100% mass) compared to silt and clay (< 60% range). SOM and bulk density, which show relatively lower performance metrics, are included to assess the model's 'lower-bound performance'. These vertical profiles were not used during model training.

In Figure 8, solid lines represent the mean soil profiles for sand content, oven-dry bulk density, and SOM across forest, cultivated crops, and wetland land use categories. Blue lines, red lines, and green lines indicate prior, observation, and posterior predictions. Comparing the solid lines, the posterior predictions align more closely with the observed data compared to the prior estimates. However, the degree of alignment varies by soil property. For sand content and SOM, the posterior predictions show better agreement with observations, while bulk density predictions exhibit greater discrepancies, particularly in cultivated areas.

For sand content, the residual correction process improves estimates, especially in wetlands, with RMSE decreasing from 7.68 to 0.77 (% mass). Bulk density predictions perform better in forested and wetland areas. In cultivated crops, the posterior predictions show larger discrepancies. This suggests that bulk density is more challenging to predict in agricultural lands, particularly in shallow layers, likely due to agricultural activities. For SOM, the residual correction effectively improves estimates, especially in the surface layers of wetlands.

Dashed lines in Figure 8 represent individual soil profiles. Prior predictions often underestimated the variability in soil properties, struggling to capture extreme values. After the residual correction, the posterior predictions are better able to approximate these extremes. However, the correction process sometimes introduces additional noise. For example, some low SOM values were generated during residual correction, even though

such values are not presented in the observed data. It is likely due to that we used the van Bemmelen factor (1.724) to convert the prior soil organic matter to soil organic carbon.

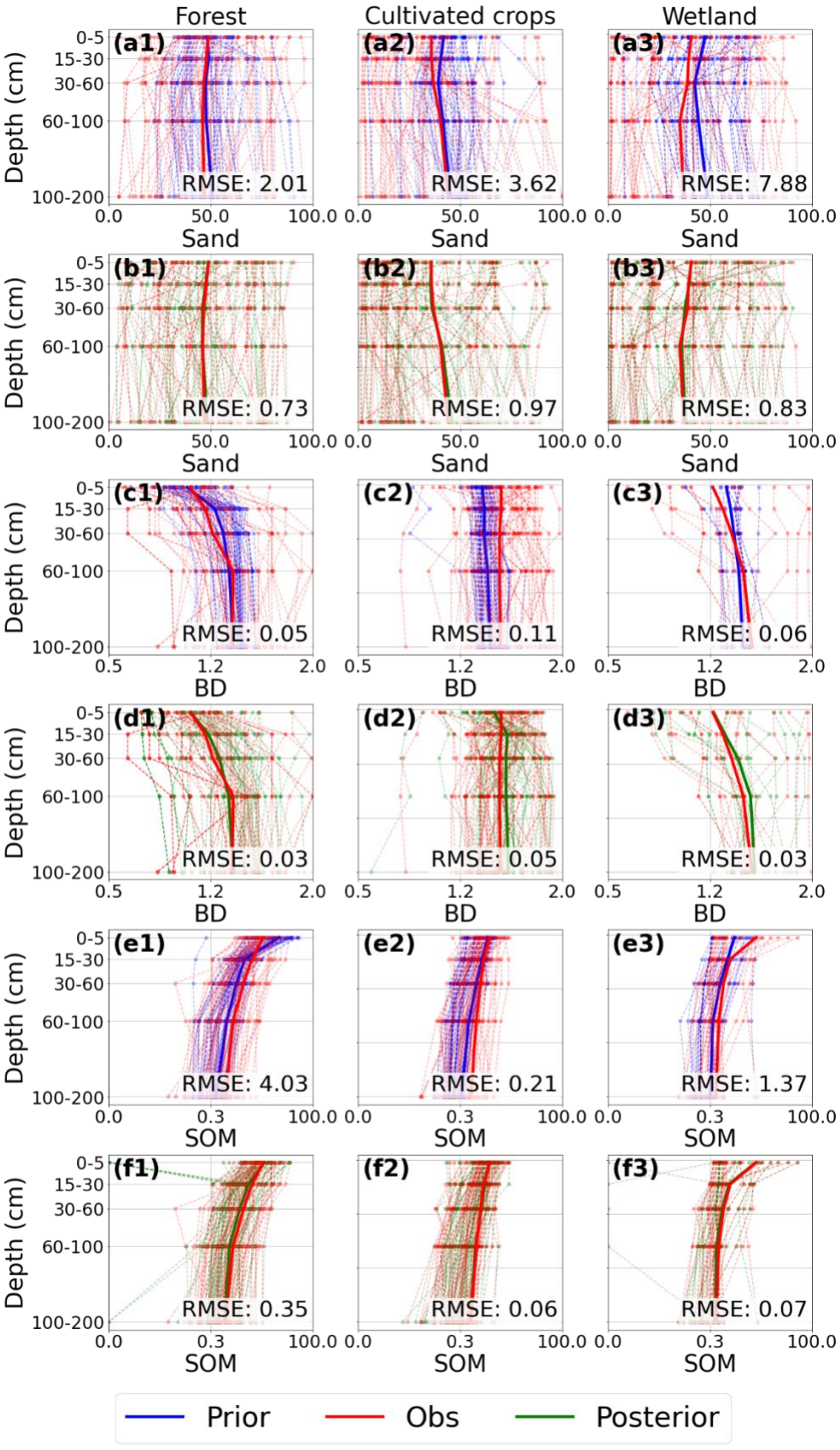
Forest
Cultivated crops
Wetland
Depth (cm)
0-5
15-30
30-60
60-100
100-200
(a1)
RMSE: 2.01
(a2)
RMSE: 3.62
(a3)
RMSE: 7.88
Sand
(b1)
RMSE: 0.73
(b2)
RMSE: 0.97
(b3)
RMSE: 0.83
(c1)
RMSE: 0.05
(c2)
RMSE: 0.11
(c3)
RMSE: 0.06
BD
(d1)
RMSE: 0.03
(d2)
RMSE: 0.05
(d3)
RMSE: 0.03
(e1)
RMSE: 4.03
(e2)
RMSE: 0.21
(e3)
RMSE: 1.37
SOM
(f1)
RMSE: 0.35
(f2)
RMSE: 0.06
(f3)
RMSE: 0.07
Prior
Obs
Posterior

642

Figure 8: Vertical distribution of soil properties (sand content, oven-dry bulk density BD, and soil organic matter SOM) across three land use categories: forest, cultivated crops, and wetland. Prior estimates (blue), posterior estimates (green), and observations (red) are shown as depth profiles. Dashed lines represent individual measurements, and solid lines show mean values. RMSE is computed elementwise to evaluate model performance across all depths. X-axis and Y-axis represent value ranges of a soil property and vertical depth intervals, respectively.

3.3 Uncertainty Analysis

Figure 9 shows the differences between 5% — 95% posterior and prior prediction interval widths (PIWs) for six soil properties—sand, silt, clay, pH, bulk density, and SOM—from surface to 2-m deep. The differences are calculated by subtracting the prior PIWs from the posteriors. Red areas present a reduction in posterior PIW, indicating the residual correction has reduced uncertainties of soil properties predictions. Blue pixels suggest the opposite. White areas represent regions where the prior and posterior uncertainties are similar.

In Figure 9, most pixels show reduced uncertainty for sand content after residual correction, particularly in agricultural and desert regions. This improvement is attributed to the inclusion of additional soil profile data from these areas. For clay content, the posterior predictions consistently show reduced uncertainty across the Sierra Nevada Mountain ranges. For SOM, the posterior PIWs improved in shallower layers (0-15 cm) over both the

Coastal Ranges and the Sierra Nevada Mountains, with the coastal line showing notably narrower PIWs. For pH, the results present a mixed pattern of PIWs after residual correction, with some areas showing reduced uncertainty and others showing the opposite. Similarly, bulk density exhibits a mixed pattern, though deeper layers (60 cm to 2 m) generally show reduced uncertainty in the Central Valley, California.

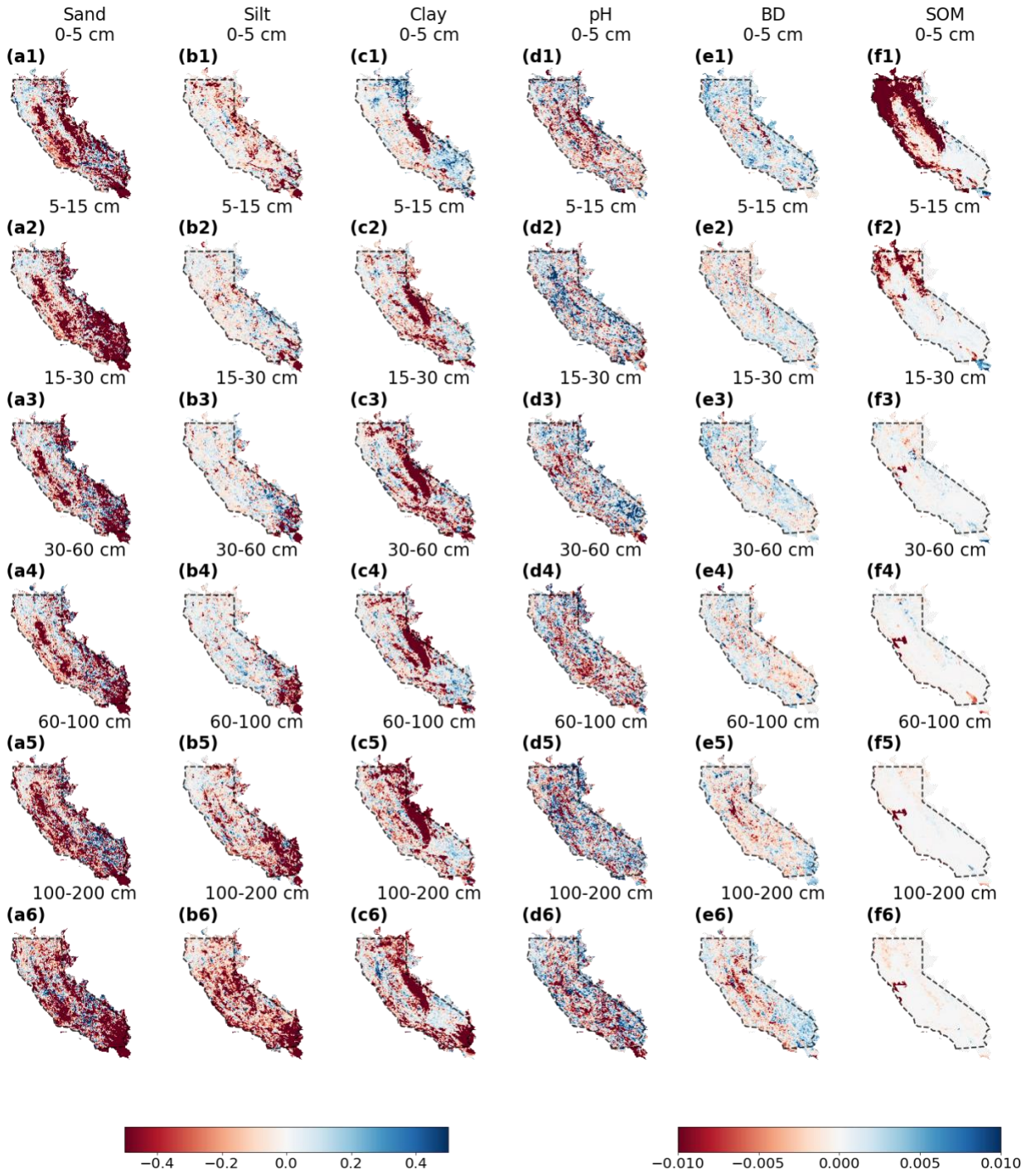

Figure 9: Differences of 5% — 95% posterior and prior prediction interval widths (PIWs) for soil properties across different depths. Each column represents a specific soil property and rows show different depths. Black polygons represent the continental part of California. Differences between posterior and prior PIWs are in a red-to-blue

color scale. Red pixels indicate a decrease in posterior PIW, indicating residual correction reduces uncertainties. Vice versa for blue pixels. White areas indicate similar extent of uncertainties. The left colorbar corresponds to sand, silt, clay with wider ranges of PIW differences. The right colorbar represents other properties with smaller PIW changes.

4 Discussion

4.1 Limitations in Soil Profile Data

The effectiveness of residual correction depends on the spatial and vertical distribution of soil profiles used to calculate residuals. In regions with sparse sampling, such as California's desert areas (Figure 1), the limited number of profiles leads to interpolating the entire area using limited observations. If soil heterogeneity is not captured by these limited samples, the residual correction would overlook it. For soil texture, most data collected by staff working on multiple projects under the National Institute of Food and Agriculture (NIFA) and the Sustainable Agricultural Systems (SAS) programs range from the surface to 1.1 meters deep (additional field measurements used in this work). We use spline interpolation to predict soil texture data beyond 1.1-m depths. It assumes vertical continuity in soil properties, which may not reflect abrupt changes in subsurface layers.

Uncertainty also arises from converting some soil organic carbon (SOC) data to soil organic matter (SOM). We used the van Bemmelen factor (1.724) to convert SOC to SOM profiles. This factor does not hold true in scenarios such as organic-rich soils. Adding data

quality controls—such as filtering profiles based on metadata (such as soil type, land use)—could filter out samples that are not suitable for this conversion. However, this conversion still has uncertainties, since even for mineral soils, this factor still has a certain extent of variation depending on the organic matter composition (lower for soils with more decomposed organic matter), soil types (forest soils or wetland soils with anaerobic decomposition), and environmental influences (such as microbial activity).

4.2 Computational Challenges

The iterative residual correction process on distributions requires computational resources, particularly when applied to large-extent or high-resolution datasets. This process involves adjusting multiple values for each pixel, as each pixel represents a distribution of soil properties. This process can be approached in two ways. The first method involves correcting the residual values for each pixel, adding these residuals to update the posterior values of soil properties, and then converting these updated values to generate a posterior distribution of soil properties. The second method first converts all pixel values into the same histogram bins and then corrects the shape of these histogram bins for each pixel. Thus, the number of values retained per pixel affects computational expense. Based on our experience, using method two, especially for soil texture, requires 100-bin histograms. Using method one with 20 most probable prior property values for residual correction can achieve comparable results while reducing memory usage.

718 The iterative process of updating features and correcting residuals also plays a role. In our
719 simulations, we observed that subsequent residual corrections generally align with
720 previous ones. To ensure consistency, we require the corrections to converge more than
721 three times across different depths. For example, residual correction for a 1-km soil
722 property map over California takes approximately two hours after preprocessing the input
723 data. However, processing higher-resolution datasets, such as those at a 10-meter scale,
724 can demand significantly more computational resources. This highlights the trade-off
725 between resolution and computational efficiency in DSM projects.
726
727 **4.3 Temporal and Spatial Constraints**
728 The current method does not account for temporal changes in soil properties, limiting its
729 applicability to dynamic properties like soil organic matter or bulk density. Incorporating
730 temporal covariates (such as seasonal land surface temperature, recent land-use
731 changes) or stratifying soil profiles by collection date could address this. However, such
732 improvements rely on the availability of temporally resolved soil data, which are often
733 limited in quantities and sampling frequency.
734
735 Spatial clustering of soil samples poses another challenge. While duplicate profiles were
736 removed during data preprocessing, nearby samples may still share a certain level of
737 similarity due to spatial autocorrelation. This could lead to overly optimistic evaluation of
738 residual correction performance. Two methods can help address this issue:

(1) Cross-validation with spatial considerations: Implement a cross-validation method for splitting training and validation sets with attention to sample locations. Ensure a minimum distance between training samples and evaluation data.

(2) Independent dataset evaluation: Use independent datasets to evaluate the model. CONUS-wide instrumental network, such as the U.S. Climate Reference Network and the National Ecological Observatory Network, provide independent soil data. However, these datasets have limitations as they were collected with clustering to certain landscapes, potentially introducing bias in the evaluation.

4.4 Similar Studies

Several continental-scale DSM products (or methods) are compared, including the Soil Survey Geographic Database (SSURGO), the Gridded National Soil Survey Geographic Database (gNATSGO), the Probabilistic Layers for the Assessment of Soils (POLARIS), Soil-Landscape Unified Synthesis (SOLUS), and the pruned Hierarchical Random Forest with iterative bias correction (pHRF with IRC) soil properties. SSURGO is a traditional, polygon-based product derived from expert field surveys and remains widely used in agricultural applications (Soil Survey Staff et al., 2023). gNATSGO mainly builds on SSURGO by rasterizing its map units to improve spatial coverage. And its estimation of soil properties still rely on utilizing metadata of legacy soil data (Soil survey staff, 2023). These two still inherit legacy data's limitations, such as scale inconsistency between soil map units and derived soil maps, inconsistencies with field observations, and report distribution of soil

761 properties with only three values (low end value, representative value, and high end value)
762 (Rossiter et al., 2022; Soil Survey Staff, 2025; Xu et al., 2025).
763
764 Development of the following DSM products incorporates quantitative models in their
765 methodology. POLARIS produces probabilistic soil property maps using machine learning
766 and the DSMART algorithm (Chaney et al., 2016, 2019; Odgers et al., 2015), while the
767 uncertainties in the DSMART algorithm can propagate into POLARIS. SOLUS integrates
768 legacy soil data with georeferenced field observations and employs linear adjusted
769 Random Forest to predict soil properties (Nauman et al., 2024). SOLUS hierarchizes soil
770 data with different qualities into its training dataset, giving more attention to georeferenced
771 observations. However, since it also uses resampled soil data derived from polygon-based
772 soil map units, this process may introduce additional uncertainties into the final product.
773 The pHRF with IRC follows a different approach. Unlike most DSM methods that directly
774 predict soil properties from input data, this approach works in two steps: first, it generates
775 a prior estimate of soil taxa and property values, then iteratively adjusts these estimates to
776 improve model performance. In future work, the pHRF with IRC method will be applied on
777 large scale and assessed with more soil properties to evaluate its generalizability.
778
779 **5 Conclusion**
780 The study introduces an iterative residual correction method for post processing used in a
781 Digital Soil Mapping (DSM) framework. The method integrates additional soil profile data
782 and iteratively optimizes the feature space to refine the distribution of soil properties until

783 the residual correction model converges. Convergence is achieved when the median
784 difference between updated and previous predictions falls below a predefined threshold,
785 ensuring consistent predictions. The proposed DSM method operates through two primary
786 steps: (1) generating prior soil property maps using the pruned hierarchical Random Forest
787 (pHRF) approach, and (2) performing iterative residual correction on the priors. Residuals
788 (differences between observed values and prior predictions) are calculated and added to
789 the prior values of soil property to adjust the statistical shape of the probability distribution
790 pixel-by-pixel. The feature space, which includes soil covariates, depth information, and
791 vertical correlations, is iteratively optimized to capture incremental adjustments to
792 subsequent predictions.
793
794 Using this method, we updated posterior distribution of soil properties for sand, silt, clay
795 content, soil pH, oven-dry bulk density, and soil organic matter over California. The results
796 show improvements in the accuracy of soil properties predictions, as shown by multiple
797 metrics including RMSE, R^2, and correlation coefficients. Furthermore, the iterative
798 residual correction model reduced prediction uncertainties, presenting narrower
799 prediction intervals compared to the priors.
800
801 Several innovations contribute to the method's improvements. First, the integration of
802 additional soil profiles allows the model to further learn from georeferenced soil
803 information, complementing prior soil property estimates derived from traditional
804 surveys. Second, the iterative update of feature space captures both spatial and vertical

soil heterogeneity through a carefully selected combination of soil covariates and vertical correlations among soil profile observations. Third, the convergence-based approach to residual correction ensures stable output of posterior predictions while avoiding overfitting since only converged residuals are added to the priors. Fourth, the implementation of physical constraints and compositional data handling maintains the realism of predicted soil properties. Future research could explore the application of this framework to other soil properties and environmental contexts, such as soil hydraulic properties and CONUS-wide simulation, to test the framework's generalization, supporting informed decision-making in soil-related applications.

Data Availability

Data will be made available on request. Code is available on https://github.com/emmaxu43/IRC_CA/tree/main.

Author Contributions

Chengcheng Xu and Nathaniel Chaney designed the study and developed the methodology. Chengcheng Xu wrote the original draft and wrote the codes to produce the methodology and analyses. Nathaniel Chaney supervised the work, provided resources and funding, and helped guide the research direction. Elia Scudiero provided funding, project management, co-supervision. Elia Scudiero and Ray Anderson provided soil property samples from California that were used as part of the input dataset. Chengcheng

Xu, Nathaniel Chaney, Elia Scudiero, and Ray Anderson discussed the results and contributed to revising and editing the manuscript.

Competing Interests

The authors declare that they have no conflict of interest.

Acknowledgements

This research was supported by the Agriculture and Food Research Initiative Competitive Grant no. 2020-69012-31914 from the USDA National Institute of Food and Agriculture. The authors want to thank Dr. Todd Skaggs for his and his teams' support for gathering input data for this work. His and Dr. Ray Anderson's efforts are supported by USDA-ARS, Office of National Programs (projects 2036-61000-019-000-D and 2036-61000-019-006-R). The U.S. Department of Agriculture prohibits discrimination in all its programs and activities on the basis of race, color, national origin, age, disability, and where applicable, sex, marital status, familial status, parental status, religion, sexual orientation, genetic information, political beliefs, reprisal, or because all or part of an individual's income is derived from any public assistance program (not all prohibited bases apply to all programs). Persons with disabilities who require alternative means for communication of program information (braille, large print, audiotape, etc.) should contact USDA's TARGET Center at (202) 720-2600 (voice and TDD). To file a complaint of discrimination, write to USDA, Director, Office of Civil Rights, 1400 Independence Avenue, S.W., Washington, D.C. 20250-9410, or call

(800) 795-3272 (voice) or (202) 720-6382 (TDD). USDA is an equal opportunity provider and employer.

Financial Support

The study was supported by USDA-NIFA-AFRI-006739 grant for sustainable agricultural systems.

References

Arrouays, D., McKenzie, N., Hempel, J., Forges, A. R. de, and McBratney, A. B.: GlobalSoilMap: Basis of the global spatial soil information system, CRC Press, 496 pp., 2014.

Batjes, N. H., Calisto, L., and de Sousa, L. M.: Providing quality-assessed and standardised soil data to support global mapping and modelling (WoSIS snapshot 2023), Earth System Science Data, 16, 4735–4765, https://doi.org/10.5194/essd-16-4735-2024, 2024.

Chaney, N. W., Wood, E. F., McBratney, A. B., Hempel, J. W., Nauman, T. W., Brungard, C. W., and Odgers, N. P.: POLARIS: A 30-meter probabilistic soil series map of the contiguous United States, Geoderma, https://doi.org/10.1016/j.geoderma.2016.03.025, 2016.

Chaney, N. W., Minasny, B., Herman, J. D., Nauman, T. W., Brungard, C. W., Morgan, C. L. S., McBratney, A. B., Wood, E. F., and Yimam, Y.: POLARIS Soil Properties: 30-m Probabilistic Maps of Soil Properties Over the Contiguous United States, Water Resources Research, https://doi.org/10.1029/2018WR022797, 2019.

Chen, C., Liaw, A., and Breiman, L.: Using random forest to learn imbalanced data, University of California, Berkeley, 110, 24, 2004.

Chilès, J.-P. and Delfiner, P.: Geostatistics: modeling spatial uncertainty, in: Geostatistics: modeling spatial uncertainty, John Wiley & Sons, Ltd, 147–237, https://doi.org/10.1002/9781118136188.ch3, 2012.

Corwin, D. L. and Scudiero, E.: Field-scale apparent soil electrical conductivity, Soil Science Society of America Journal, 84, 1405–1441, https://doi.org/10.1002/saj2.20153, 2020.

Grunwald, S., Thompson, J. A., and Boettinger, J. L.: Digital Soil Mapping and Modeling at Continental Scales: Finding Solutions for Global Issues, Soil Science Society of America Journal, 75, 1201–1213, https://doi.org/10.2136/SSSAJ2011.0025, 2011.

Haghverdi, A., Najarchi, M., öztürk, H. S., and Durner, W.: Studying unimodal, bimodal, PDI and bimodal-PDI variants of multiple soil water retention models: I. Direct model fit using the extended evaporation and dewpoint methods, Water (Switzerland), 12, https://doi.org/10.3390/w12030900, 2020.

Hartemink, A. E., Hempel, J., Lagacherie, P., McBratney, A., McKenzie, N., MacMillan, R. A., Minasny, B., Montanarella, L., de Mendonça Santos, M. L., Sanchez, P., Walsh, M., and Zhang, G.-L.: GlobalSoilMap.net – A New Digital Soil Map of the World, in: Digital Soil Mapping: Bridging Research, Environmental Application, and Operation, edited by: Boettinger, J. L., Howell, D. W., Moore, A. C., Hartemink, A. E., and Kienast-Brown, S., Springer Netherlands, Dordrecht, 423–428, https://doi.org/10.1007/978-90-481-8863-5_33, 2010.

Hengl, T., Heuvelink, G. B., and Stein, A.: A generic framework for spatial prediction of soil variables based on regression-kriging, Geoderma, 120, 75–93, 2004.

Hengl, T., De Jesus, J. M., Heuvelink, G. B. M., Gonzalez, M. R., Kilibarda, M., Blagotić, A., Shangguan, W., Wright, M. N., Geng, X., Bauer-Marschallinger, B., Guevara, M. A., Vargas, R., MacMillan, R. A., Batjes, N. H., Leenaars, J. G. B., Ribeiro, E., Wheeler, I., Mantel, S., and Kempen, B.: SoilGrids250m: Global gridded soil information based on machine learning, PLoS ONE, https://doi.org/10.1371/journal.pone.0169748, 2017.

Jiang, Q., Fu, Q., and Wang, Z.: Delineating site-specific irrigation management zones, Irrigation and Drainage, 60, 464–472, https://doi.org/10.1002/ird.588, 2011.

Lesch, S., Rhoades, J., and Corwin, D.: ESAP-95 version 2.01 R: User manual and tutorial guide, Research Rpt, 146, 17, 2000.

Lesch, S. M.: Sensor-directed response surface sampling designs for characterizing spatial variation in soil properties, Computers and Electronics in Agriculture, 46, 153–179, https://doi.org/10.1016/j.compag.2004.11.004, 2005.

Li, N., Zhao, X., Wang, J., Sefton, M., and Triantafilis, J.: Digital soil mapping based site-specific nutrient management in a sugarcane field in Burdekin, Geoderma, 340, 38–48, https://doi.org/10.1016/j.geoderma.2018.12.033, 2019.

McBratney, A. B., Mendonça Santos, M. L., and Minasny, B.: On digital soil mapping, Geoderma, 117, 3–52, https://doi.org/10.1016/S0016-7061(03)00223-4, 2003.

Minasny, B. and McBratney, A. B.: A conditioned Latin hypercube method for sampling in the presence of ancillary information, Computers & geosciences, 32, 1378–1388, 2006.

Mueller, T. G., Pierce, F. J., Schabenberger, O., and Warncke, D. D.: Map Quality for Site-Specific Fertility Management, Soil Science Society of America Journal, 65, 1547–1558, https://doi.org/10.2136/sssaj2001.6551547x, 2001.

National Cooperative Soil Survey: NCSS Soil Characterization Database (Lab Data Mart), 2018.

Nauman, T. W., Kienast-Brown, S., Roecker, S. M., Brungard, C., White, D., Philippe, J., and Thompson, J. A.: Soil landscapes of the United States (SOLUS): Developing predictive soil property maps of the conterminous United States using hybrid training sets, Soil Science Society of America Journal, 88, 2046–2065, https://doi.org/10.1002/saj2.20769, 2024.

Nussbaum, M., Zimmermann, S., Walthert, L., and Baltensweiler, A.: Benefits of hierarchical predictions for digital soil mapping—An approach to map bimodal soil pH, Geoderma, 437, 116579, https://doi.org/10.1016/j.geoderma.2023.116579, 2023.

Odgers, N. P., McBratney, A. B., and Minasny, B.: Digital soil property mapping and uncertainty estimation using soil class probability rasters, Geoderma, 237, https://doi.org/10.1016/j.geoderma.2014.09.009, 2015.

Oliver, M. A. and Webster, R.: A tutorial guide to geostatistics: Computing and modelling variograms and kriging, CATENA, 113, 56–69, https://doi.org/10.1016/j.catena.2013.09.006, 2014.

Ortuani, B., Chiaradia, E. A., Priori, S., L'Abate, G., Canone, D., Comunian, A., Giudici, M., Mele, M., and Facchi, A.: Mapping Soil Water Capacity Through EMI Survey to Delineate Site-Specific Management Units Within an Irrigated Field, Soil Science, 181, 252, https://doi.org/10.1097/SS.0000000000000159, 2016.

Poggio, L., De Sousa, L. M., Batjes, N. H., Heuvelink, G. B. M., Kempen, B., Ribeiro, E., and Rossiter, D.: SoilGrids 2.0: Producing soil information for the globe with quantified spatial uncertainty, SOIL, 7, 217–240, https://doi.org/10.5194/SOIL-7-217-2021, 2021.

Powers, J. S., Corre, M. D., Twine, T. E., and Veldkamp, E.: Geographic bias of field observations of soil carbon stocks with tropical land-use changes precludes spatial extrapolation, Proceedings of the National Academy of Sciences, 108, 6318–6322, https://doi.org/10.1073/pnas.1016774108, 2011.

Ramcharan, A., Hengl, T., Nauman, T., Brungard, C., Waltman, S., Wills, S., and Thompson, J.: Soil Property and Class Maps of the Conterminous United States at 100-Meter Spatial Resolution, Soil Science Society of America Journal, 82, 186–201, https://doi.org/10.2136/sssaj2017.04.0122, 2018.

Rossiter, D. G., Poggio, L., Beaudette, D., and Libohova, Z.: How well does digital soil mapping represent soil geography? An investigation from the USA, SOIL, 8, 559–586, https://doi.org/10.5194/soil-8-559-2022, 2022.

947 Schmidinger, J. and Heuvelink, G. B. M.: Validation of uncertainty predictions in digital soil
948 mapping, Geoderma, 437, 116585, https://doi.org/10.1016/j.geoderma.2023.116585,
949 2023.

950 Scudiero, E., Corwin, D. L., Markley, P. T., Pourreza, A., Rounsaville, T., Bughici, T., and
951 Skaggs, T. H.: A system for concurrent on-the-go soil apparent electrical conductivity and
952 gamma-ray sensing in micro-irrigated orchards, Soil and Tillage Research, 235, 105899,
953 2024.

954 Sharififar, A., Sarmadian, F., Malone, B. P., and Minasny, B.: Addressing the issue of digital
955 mapping of soil classes with imbalanced class observations, Geoderma, 350, 84–92,
956 https://doi.org/10.1016/j.geoderma.2019.05.016, 2019.

957 Shi, G., Sun, W., Shangguan, W., Wei, Z., Yuan, H., Zhang, Y., Liang, H., Li, L., Sun, X., Li, D.,
958 Huang, F., Li, Q., and Dai, Y.: A China dataset of soil properties for land surface modeling
959 (version 2), https://doi.org/10.5194/essd-2024-299, 29 August 2024.

960 Soil, K.: Survey laboratory methods manual, Soil Survey Investigations Report, 1996.

961 Soil Survey Staff: Kellogg Soil Survey Laboratory methods manual, U.S. Department of
962 Agriculture, Natural Resources Conservation Service, Lincoln, Nebraska, 2014.

963 Soil survey staff: Gridded National Soil Survey Geographic (gNATSGO) Database for the
964 Conterminous United States, 2023. Natural Resources Conservation Service, United
965 States Department of Agriculture.

966 Soil Survey Staff: Gridded Soil Survey Geographic (gSSURGO) Database for the
967 Conterminous United States, 2025. Natural Resources Conservation Service, United
968 States Department of Agriculture.

969 Soil Survey Staff, Natural Resources Conservation Service, and United States Department
970 of Agriculture: Soil Survey Geographic (SSURGO) Database for the CONUS, 2023. Natural
971 Resources Conservation Service, United States Department of Agriculture.

972 Sylvain, J.-D., Anctil, F., and Thiffault, É.: Using bias correction and ensemble modelling for
973 predictive mapping and related uncertainty: A case study in digital soil mapping,
974 Geoderma, 403, 115153, https://doi.org/10.1016/j.geoderma.2021.115153, 2021.

975 Takoutsing, B., Heuvelink, G. B. M., Stoorvogel, J. J., Shepherd, K. D., and Aynekulu, E.:
976 Accounting for analytical and proximal soil sensing errors in digital soil mapping, European
977 Journal of Soil Science, 73, e13226, https://doi.org/10.1111/ejss.13226, 2022.

978 Vereecken, H., Schnepf, A., Hopmans, J. W., Javaux, M., Or, D., Roose, T., Vanderborght, J.,
979 Young, M. H., Amelung, W., Aitkenhead, M., Allison, S. D., Assouline, S., Baveye, P., Berli,
980 M., Brüggemann, N., Finke, P., Flury, M., Gaiser, T., Govers, G., Ghezzehei, T., Hallett, P.,
981 Hendricks Franssen, H. J., Heppell, J., Horn, R., Huisman, J. A., Jacques, D., Jonard, F.,

Kollet, S., Lafolie, F., Lamorski, K., Leitner, D., McBratney, A., Minasny, B., Montzka, C., Nowak, W., Pachepsky, Y., Padarian, J., Romano, N., Roth, K., Rothfuss, Y., Rowe, E. C., Schwen, A., Šimůnek, J., Tiktak, A., Van Dam, J., van der Zee, S. E. A. T. M., Vogel, H. J., Vrugt, J. A., Wöhling, T., and Young, I. M.: Modeling Soil Processes: Review, Key Challenges, and New Perspectives, Vadose Zone Journal, 15, vzj2015.09.0131, https://doi.org/10.2136/vzj2015.09.0131, 2016.

Vereecken, H., Amelung, W., Bauke, S. L., Bogena, H., Brüggemann, N., Montzka, C., Vanderborght, J., Bechtold, M., Blöschl, G., Carminati, A., Javaux, M., Konings, A. G., Kusche, J., Neuweiler, I., Or, D., Steele-Dunne, S., Verhoef, A., Young, M., and Zhang, Y.: Soil hydrology in the Earth system, Nat Rev Earth Environ, 3, 573–587, https://doi.org/10.1038/s43017-022-00324-6, 2022.

Wu, Y., Huang, Y., Chen, Z., Yao, Z., Fu, Y., Liu, K., Luo, X., and Wang, D.: Iterative Feature Space Optimization through Incremental Adaptive Evaluation, https://doi.org/10.48550/arXiv.2501.14889, 24 January 2025.

Xu, C., Huang, J., Hartemink, A. E., and Chaney, N. W.: Pruned hierarchical Random Forest framework for digital soil mapping: Evaluation using NEON soil properties, Geoderma, 459, 117392, https://doi.org/10.1016/j.geoderma.2025.117392, 2025.

Zhang, G. and Lu, Y.: Bias-corrected random forests in regression, Journal of Applied Statistics, 39, 151–160, https://doi.org/10.1080/02664763.2011.578621, 2012.